Clouds and radiatively induced circulations

Tra Dinh[1,*], Blaž Gasparini[2], and Gilles Bellon[1]

[1]*Department of Physics, University of Auckland, Auckland, New Zealand*
[2]*Department of Meteorology and Geophysics, University of Vienna, Vienna, Austria*
[*]*Corresponding author: Tra Dinh, t.dinh@auckland.ac.nz*

In the atmosphere, there is an intimate relationship between clouds, atmospheric radiative cooling/heating, and radiatively induced circulations at various temporal and spatial scales. This coupling remains not well understood, which contributes to limiting our ability to model and predict clouds and climate accurately.

Cloud liquid and ice particles interact with both shortwave (SW) and longwave (LW) radiation, leading to cloud radiative effect (CRE). The CRE includes perturbations of the radiative fluxes at the top of the atmosphere (TOA) and the surface, as well as perturbations of the radiative cooling profile within the atmosphere. The effect of clouds that results in atmospheric radiative heating or cooling that is distinct from the clear-sky radiative cooling profile will be termed the CRE on atmospheric heating, or CRE-AH. The CRE-AH can significantly modify the horizontal and vertical gradients of the diabatic heating profile, inducing circulations at various scales in the atmosphere. In turn, circulations govern cloud formation and evolution processes and therefore the properties and distribution of clouds.

This chapter explores advances in research of the coupling between clouds and radiatively induced circulations and identify the paths forward. The chapter is organized into three sections. Section 1 discusses the relationship between clouds and tropospheric diabatic circulations in which condensate and precipitation are produced. Section 2 focuses on low clouds and shallow radiatively induced circulations in the boundary layer and lower free troposphere. Section 3 focuses on tropical high clouds and the circulations induced by the CRE-AH in these clouds. All the radiatively induced circulations discussed in the three sections are illustrated in Fig. 1.

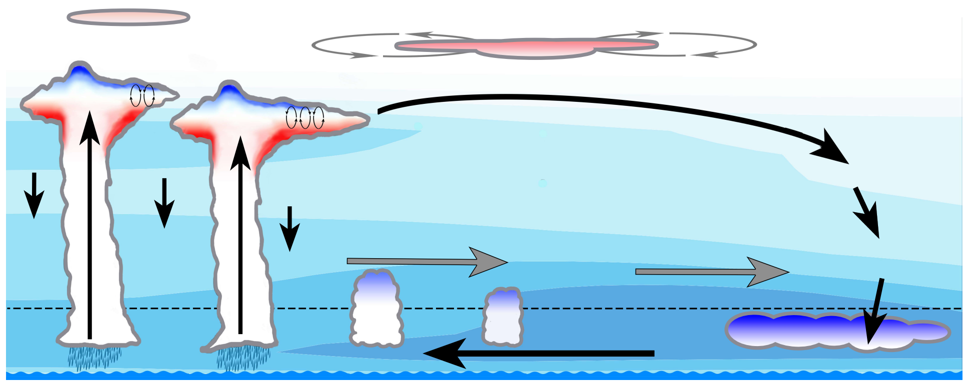

Figure 1: Illustration of the radiatively induced circulations discussed in this chapter, including tropospheric diabatic circulations (thick, black arrows, see Section 1), large-scale shallow circulations (thick, black arrows in the boundary layer and thick, grey arrows in the lower free troposphere, see Section 2), mesoscale circulations of tropical high clouds (thin, grey arrows, see Section 3), and small-scale convective motions within the anvils (thin, black arrows, see Section 3). The thin, dashed line marks the top of the boundary layer, which is located at altitudes of about 1–2 km. The background shading represents the clear-sky radiative cooling. The shading within the clouds indicates the CRE-AH. Blue indicates radiative cooling and red indicates radiative heating.

1 Clouds and tropospheric diabatic circulations

The relationship between clouds and tropospheric diabatic circulations is two-way. On the one hand, clouds are formed in the atmosphere as water vapor condenses within the moist, convective branch of these diabatic circulations. On the other hand, the perturbation in the diabatic heating profile due to the CRE-AH can feed back on to weaken or strengthen the circulations in which clouds form and evolve. In this section, we will review progresses in our understanding of this coupling, particularly in the context of the tropospheric diabatic circulations that underlie the atmospheric water cycle.

Following directly from the fact that cloud condensates are produced within the atmospheric water cycle, understanding of cloud behaviors may be obtained by studying the atmospheric water cycle. As a metric of the strength of the atmospheric water cycle, let us use the rate of condensation of water vapor in the atmosphere, i.e. the rate (in $\mathrm{kg\,kg^{-1}\,s^{-1}}$) at which water vapor is transformed into condensate at a given location in the atmosphere. The condensation rate by itself does not dictate the percentage of condensates that remain in the atmosphere as clouds rather than falling to the surface as precipitation. But, if we assume that the percentage of cloud condensates (out of the total condensates) does not change under small perturbations of the climate, we will be able to obtain a first-order constraint on clouds based on the constraint on the condensation rate.

To formulate a constraint on the condensation rate—hereafter denoted by m_{cond}, we consider the moisture budget in the atmosphere following Schneider et al. (2010). In the free troposphere, a balanced water vapor budget in steady state is maintained between condensation and vertical advection of water vapor, i.e.

$$[m_{\mathrm{cond}}] = -[\omega \partial_p q], \tag{1}$$

where ω is the pressure velocity, p is pressure, and q is the specific humidity. The notation $[\cdot]$ indicates that the variable between the brackets is averaged horizontally over a sufficiently large domain for which horizontal advection of water vapor into/out of the domain can be neglected. The entire globe and the tropics are examples of such a domain. Equation (1) however applies only to the free troposphere; in the boundary layer, the source of moisture that results from surface evaporation must be considered. Below, we will first focus on the free troposphere and then touch upon the complications of the boundary layer toward the end of the section.

In a moist convecting atmosphere, vertical advection of water vapor is upward and mostly carried out by moist convection. The updrafts inside moist convective regions are saturated with water vapor above the lifted condensation level (LCL). Thus,

$$[m_{\mathrm{cond}}] \sim -[\omega_{\uparrow}\partial_p q_{\mathrm{sat}}]_{\mathrm{conv}} \sim -[\omega_{\uparrow}]_{\mathrm{conv}}[\partial_p q_{\mathrm{sat}}]_{\mathrm{conv}} \tag{2}$$

above the LCL (c.f. Eq. 5 in Schneider et al., 2010). Here q_{sat} is the saturation specific humidity, $\omega_{\uparrow}$ is the upward component of the pressure velocity, and $[\cdot]_{\mathrm{conv}}$ indicates that the variable between the square brackets is averaged over moist convective regions within the domain only.

Over this domain, an overturning diabatic circulation can be constructed as consisting of a moist ascending branch in which latent heat is released as water vapor condenses forming condensates and precipitation (see the upward arrows in the deep convective clouds in Fig. 1) and a dry descending branch regulated by radiative cooling (see the downward arrows in clear air in Fig. 1). A nice illustration of such an overturning diabatic circulation is Fig. 10.3 in Wallace and Hobbs (2006). Following Yano et al. (2002), Zelinka and Hartmann (2010), Bony et al. (2016), Dinh and Fueglistaler (2017, 2019), we seek to estimate the convective mass flux $[\omega_{\uparrow}]_{\mathrm{conv}}$ as

$$[\omega_{\uparrow}]_{\mathrm{conv}} \sim -[\omega_{\mathrm{rad}}], \tag{3}$$

where

$$[\omega_{\mathrm{rad}}] \sim \frac{[Q_{\mathrm{rad}}]}{[\sigma]} \tag{4}$$

is the radiative subsidence mass flux, Q_{rad} is the radiative cooling rate, σ is the static stability, and T is atmospheric temperature. Furthermore, by assuming that the saturation specific humidity within moist convective regions scales with the domain average profile ($[\partial_p q_{\mathrm{sat}}]_{\mathrm{conv}} \sim [\partial_p q_{\mathrm{sat}}]$), we obtain

$$[m_{\mathrm{cond}}] \sim \frac{[\partial_p q_{\mathrm{sat}}]}{[\sigma]}[Q_{\mathrm{rad}}]. \tag{5}$$

Equation (5) indicates that the condensation rate depends on the radiative cooling rate as well as the factor

$$[f] = \frac{[\partial_p q_{\mathrm{sat}}]}{[\sigma]}, \tag{6}$$

which is a function of atmospheric temperature. The atmospheric water cycle can be considered as driven by atmospheric radiative cooling, but processes that affect the vertical profile of temperature can affect the condensation rate and potentially clouds as well.

The linkage between tropospheric diabatic circulations and clouds as outlined above has been used to explain how clouds would change following an increase in atmospheric CO_2 concentration and subsequent global warming. The responses of the water cycle and clouds to the radiative forcing from CO_2 increase consist of two components (Dinh and Fueglistaler, 2017): (i) rapid adjustment (Gregory et al., 2004) which occurs in the atmosphere independently of surface temperature changes and (ii) a slower response that follows surface warming. Climate models consistently predict that global precipitation and cloud water decrease during rapid atmospheric adjustment (see Dinh and Fueglistaler, 2019 and references therein). Dinh and Fueglistaler (2019) explained that the weakening of the atmospheric water cycle and decrease in cloud water are driven by the decrease in atmospheric radiative cooling, a direct result of the CO_2 increase. Atmospheric radiative cooling decreases because the added CO_2 enhances the total atmospheric absorption of the LW radiation emitted by the surface. On the other hand, the slow response following surface warming shows increases in tropical rain rate and high cloud water content (Larson and Hartmann, 2003). These changes under warming are driven by an increase in atmospheric radiative cooling, which is largely associated with increased water vapor and increased emission of LW radiation by water vapor at higher atmospheric temperatures. Further research is needed to confirm whether the increase in cloud water holds globally and to investigate the differences in the responses of tropical and extra-tropical clouds to warming.

The radiative cooling constraint on tropospheric diabatic circulations has been shown useful in evaluating the radiative climate feedback of tropical high clouds. Given that the convective mass flux is constrained by the radiative cooling ($[Q_{\rm rad}]$) following Eqs. (3) and (4), it can be expected that tropical convection and convective anvil clouds detrain near the level in the upper troposphere where $[Q_{\rm rad}]$ decreases rapidly with height. For the Earth's atmosphere, $[Q_{\rm rad}]$ is governed to a large extent by water vapor, whose vertical profile and radiative effect depend strongly on atmospheric temperature. Hartmann and Larson (2002) therefore proposed that the atmospheric temperature at which the LW radiative emission and atmospheric radiative cooling by water vapor become inefficient remains the same regardless of surface temperature. It follows that the temperature at the detrainment level and therefore the emission temperature of tropical anvil clouds remain constant as the surface warms; the clouds absorb more upwelling LW radiation from a warming surface and atmosphere below but emit the same amount of LW radiation. This "fixed anvil temperature" (FAT) hypothesis therefore implies a positive climate feedback of tropical anvil clouds.

The original FAT hypothesis does not account for the increased static stability ($[\sigma]$) at the level where $[Q_{\text{rad}}]$ decreases rapidly with height. In a follow-up work, Zelinka and Hartmann (2010) calculated the convergence profile of tropical tropospheric diabatic circulations from the vertical gradient of $[\omega_{\text{rad}}]$ using the clear-sky $[Q_{\text{rad}}]$ profile (see Eq. 4). They found that the peak of the convergence profile shifts upward as the surface warms, consistently with the upward shift of the clear-sky $[Q_{\text{rad}}]$. However, the peak convergence level warms slightly and correspondingly the anvil cloud temperature increases slightly as the static stability at this level increases. These findings confirm that the climate feedback of tropical anvil clouds is positive but of a smaller magnitude than that suggested by the original FAT hypothesis.

Using the same argument, Bony et al. (2016) proposed that tropical anvil cloud cover is expected to shrink under warming. As the climate warms, the anvil clouds rise to remain at approximately the same temperature following the FAT hypothesis. As the clouds rise they are embedded in a more stable atmosphere. The increased stability decreases the radiatively driven mass flux (see Eq. 4) and the convective outflow, leading to a reduction of the anvil cloud fraction. This stability effect has been confirmed based on interannual variations of anvil cloud fraction (Saint-Lu et al., 2020) in data from the Cloud-Aerosol Lidar and Infrared Pathfinder Satellite Observations (CALIPSO).

The original FAT hypothesis was developed for the tropics only, but the same general behavior of atmospheric radiative cooling, which is dominated by water vapor, also holds in the extra-tropics (Thompson et al., 2017). The pressure level in the upper troposphere at which the clear-sky atmospheric radiative cooling profile decreases rapidly with height thus defines the top of the troposphere and cloud-top temperature throughout the globe. This is a strong constraint that can be used to infer cloud top height and how it changes under warming.

Much of the discussions above have focused on the aspect of the circulation–cloud coupling which concerns how the atmospheric water cycle governs large-scale cloudiness. Let us now address the second aspect of this coupling which concerns how the CRE-AH—through its impact on atmospheric radiative cooling—feeds back on diabatic circulations. Referring again to Eq. (5), we see that the CRE-AH can affect the condensation rate and therefore precipitation either by directly modifying the radiative cooling profile or by indirectly modifying the temperature profile through the radiative cooling perturbation. The temperature profile governs both the vertical gradient of the saturation specific humidity and the static stability in the atmosphere, which are the numerator and denominator of the factor $[f]$ defined in Eq. (6).

A number of studies using numerical simulations have shown that the CRE-AH plays an important role in determining the mean tropical circulation (Slingo and Slingo, 1988, 1991, Bergman and Hendon, 2000, Tian and Ramanathan, 2003) as well as the general circulation of the atmosphere and global precipitation (Randall et al., 1989, Li et al., 2015). Averaged over the tropics and/or globally, the CRE-AH produces radiative heating in the free troposphere, correspondingly a reduction in the all-sky radiative cooling rate (see e.g. Fig. 4 in Li et al., 2015). If this were the only effect of the CRE-AH, we would expect that precipitation decreases—particularly in the tropics where the reduction in the radiative cooling rate by the CRE-AH is largest. However, in all of the aforementioned studies but Li et al. (2015), it was found on the contrary that the CRE-AH enhances precipitation. Randall et al. (1989) found that the CRE-AH results in a warmer and deeper troposphere. When integrated over a warmer and deeper troposphere, the $[\partial_p q_{\text{sat}}]$ term in Eq. (5) increases significantly. An enhancement in precipitation thus occurs despite reduced radiative cooling.

Given that the role of the CRE-AH on diabatic circulations remains inconclusive, it would be worthwhile to re-examine this topic in future studies. For future analysis, the impact of the CRE-AH on precipitation can be evaluated more accurately by accounting for all of the three terms $[Q_{\text{rad}}]$, $[\partial_p q_{\text{sat}}]$, and $[\sigma]$ in Eq. (5). Above we have touched upon the impacts of the CRE-AH on $[Q_{\text{rad}}]$ and $[\partial_p q_{\text{sat}}]$, but the CRE-AH also affects $[\sigma]$—both locally by modifying the vertical profile of temperature in cloudy air and remotely by modifying the meridional temperature gradient. As shown in Li et al. (2015), the difference in the CRE-AH between the tropics and the extra-tropics leads to a meridional temperature gradient that affects the meridional transport of energy by the eddies. The transport of energy by the eddies in turn affects the static stability in the extra-tropics.

The discussions so far have been limited to clouds in the free troposphere above the boundary layer. Strictly speaking, the scaling argument used previously for the free troposphere (see Eqs. 1–6) does not apply to the boundary layer because (i) the source of moisture that results from surface evaporation must be added to the moisture budget balance in Eq. (1) for the boundary layer and (ii) the updrafts in the boundary layer below the LCL are not saturated. Nevertheless, in the upper boundary layer, the impact of clouds on large-scale diabatic circulations can be qualitatively understood from the radiative cooling constraint. In the upper boundary layer (around 750–850 hPa), the CRE-AH is dominated by the LW emission by cloud hydrometeors, leading to enhanced radiative cooling there (Haynes et al., 2013). This effect is apparent in the prevalent marine stratocumulus in the subtropics and higher latitudes (Wood, 2012). The CRE-AH of boundary layer clouds thus strengthens the overturning diabatic circulations, resulting in an increase in the globally averaged precipitation (Fermepin and Bony, 2014). For other issues regarding the coupling between radiatively induced circulations and low clouds, the readers are referred to Section 2 below.

In summary, notable progress in our understanding of the coupling between circulations and clouds has been made in the last few decades. In particular, constraints on how clouds change under climate change have been obtained based on basic understanding of tropospheric diabatic circulations. These constraints on cloud properties (vertical and horizontal distributions, water content, and coverage) will enable improved, accurate evaluation of the impacts of the CRE on the Earth's energy budget and the climate feedback of clouds on global warming. However, existing studies have not settled on the roles of the CRE-AH on circulations and precipitation. This leaves significant opportunities for future studies. Progress is anticipated to occur rapidly within the next decade given the advancement in model development and increasing availability of global and long-term observational data of clouds (such as CALIPSO).

2 Low clouds and shallow circulations

Shallow circulations are characterized by a convergence/divergence in the boundary layer and a compensating flow in the lower free troposphere. The ascending branch of these circulations is generally located in the warm, convective regions and the descending branch in the cooler, less convective regions because of the pressure gradients created by the temperature anomalies. Boundary layer convergence occurs in the warm, convective regions and divergence in the cool, non-convective regions (see the horizontal black arrow near the bottom of Fig. 1), with opposite patterns just above the boundary layer (see the horizontal grey arrows in Fig. 1). Shallow circulations appear in numerical model simulations at both mesoscale and large scales and have been observed in the tropics at large scales. In this section, we will first explain the mechanism that gives rise to such circulations. Second, we will review how these circulations influence the spatial organization of convection. Lastly, we will review the instances of observed shallow circulations and their influence on the large-scale tropical climatology.

2.1 Mechanism of shallow circulations

In non-convective regions, the boundary layer experiences radiative cooling at its top, mostly through LW radiation. This cooling results from both low clouds and clear-sky processes. Indeed, the boundary layer is significantly moister, and therefore absorbs and re-emits more LW radiation than the free troposphere above. A large part of the LW radiation emitted upward at the top of the boundary layer is not absorbed by the free troposphere and hence escapes to space, allowing the boundary layer top to cool. Cloud hydrometeors also absorb and emit infrared radiation very efficiently, so low clouds experience strong radiative cooling at their tops as well. This cooling is particularly intense in the case of stratocumulus clouds (Wood, 2012, Bellon and Geoffroy, 2016, Bellon and Bony, 2020). Mixing by turbulence redistributes the cooling from the top of the boundary layer downward. Vertical turbulent mixing is very efficient in a well-mixed boundary layer but a little less so in a shallow convective boundary layer.

The radiative cooling in the boundary layer can give rise to shallow circulations. In the hydrostatic approximation,

$$\frac{\partial \Phi}{\partial p} = -\frac{1}{\rho} \approx -\frac{R_{\mathrm{a}} T}{p} \tag{7}$$

with Φ the geopotential, ρ the density, T the temperature, p the pressure, and R_{a} the specific gas constant of air. This means that the vertical increase of the geopotential through the boundary layer is smaller in radiatively cooled regions than in others. The baroclinic component of this pattern corresponds to the geopotential near the surface being larger in radiatively cooled regions than in others, and the geopotential at the top of the boundary layer being smaller in these cooled regions than in others. The associated geopotential gradient forces a circulation that includes outflow of air from the cooled regions in the boundary layer and inflow of air toward the cooled regions just above the boundary layer. This mechanism has been illustrated and validated by Large Eddy Simulation experiments and conceptual models (Naumann et al., 2017, 2019).

2.2 Shallow circulations and aggregation of convection

Shallow circulations differ from troposphere-deep circulations particularly in terms of the transport of moist static energy (MSE) $h = c_{\mathrm{p}} T + \Phi + L_{\mathrm{v}} q$, with

c_p the specific heat capacity of air at constant pressure, L_v the latent heat of vaporization, and q the specific humidity. Shallow circulations transport MSE up-gradient and therefore increase the contrast in MSE between the convective and dry regions, while deep circulations transport MSE down-gradient and reduce such contrast.

The difference in the direction of transport of MSE between troposphere-deep circulations and shallow circulations results from the stratification of MSE in the atmosphere: h is large in the boundary layer where the humidity is high, minimum in the lower free troposphere where the humidity is low, and monotonically increases with altitude in the free troposphere because of the contribution from the geopotential; at the tropopause it reaches values similar to the surface values (see Fig. 4 in Glenn and Krueger, 2017). The vertical integral of h over the middle and upper troposphere is larger than the vertical integral of h over the boundary layer. Therefore, the upper branches of troposphere-deep circulations transport more MSE (from the ascending regions into the subsiding regions) than their lower branches in the boundary layer (from the subsiding regions into the ascending regions). The net effect is that troposphere-deep circulations export MSE from ascending, convective regions of large column-integrated MSE to dry, subsiding regions with small column-integrated MSE. In contrast, shallow circulations import MSE from their subsiding branches (where column-integrated MSE is small) into their ascending branches (where column-integrated MSE is large).

Because shallow circulations increase the horizontal gradient of MSE, they create a positive feedback on the spatial variability: anomalies in MSE are reinforced by the transport associated with these circulations. As a result, shallow circulations can be powerful actors in the spatial organization of convection: warm, convective regions become warmer and moister while dry, cool regions become cooler and drier. This mechanism of spatial organization of convection, named “self-aggregation” is documented both in convection-permitting simulations and in general circulation model (GCM) simulations even without any external circulation nor the effect of rotation. In particular, low-level radiative cooling can cause the development of cooler and drier regions, sometimes called “radiative cold pools” that are instrumental to the development of self-aggregation. Figures 2 and 3 show examples of such radiative cold pools in a convection-permitting model and a GCM.

Figure 2 shows results of an idealized simulation (see Bellon and Coppin, 2021) using the non-hydrostatic mesoscale model MesoNH (Lafore et al., 1998, Lac et al., 2018) in a convection-permitting configuration. The domain is $90\,000\,\mathrm{km}^2$ with a 3-km horizontal resolution and 48 vertical levels. The configuration prescribes a fixed sea surface temperature of 301 K over the entire domain and a horizontally uniform large-scale subsidence ($0.5\,\mathrm{kg\,m^{-2}\,s^{-1}}$ at 400 hPa). Figure 2 shows the average variables over one day of the stationary state reached in this simulation.

Figure 2(a) shows the horizontal distribution of precipitable water in the MesoNH simulation described above, with a clear dry patch surrounded by a fairly uniform moist region. Using the bimodality of the distribution of column-integrated MSE, a dry region and a moist region can objectively be identified and the dashed line in Fig. 2(a) shows the boundary between these regions. Figures 2(b) and (c) show the vertical profiles of the mixing ratios of water vapor and cloud condensates averaged over each of these regions. The figures show that the dry column is much drier than the moist column, both in the boundary layer and in the free troposphere, and with hardly any clouds. The moist region is convective, with large amount of cloud condensates throughout the troposphere.

Figure 2(d) shows the radiative heating rates (with negative values indicating radiative cooling) in the dry and moist regions. In the lower troposphere, the LW radiative cooling is larger in the dry region because of the smaller greenhouse effect of water vapor and clouds in the free troposphere above. Conversely, in the upper troposphere, the LW radiative cooling is larger in the moist region because of the re-emission of terrestrial radiation by the large amount of water vapor and clouds there. Except in the boundary layer, the SW radiative heating is larger in the moist region where there is more absorption of solar radiation by water vapor and clouds. The difference is opposite in the boundary layer because the downward solar radiative flux reaching the top of the boundary layer is larger in the dry region. In this simulation, the differences in the LW and SW effects compensate each other in the upper troposphere, but not in the lower troposphere where the net radiative cooling is larger (by about $0.5\,\mathrm{K\,d^{-1}}$) in the dry region than in the moist region. The radiative cooling of the dry region relative to the moist region creates a shallow circulation with winds diverging from the dry region near the surface and a return flow in the lower free troposphere. Consistently with the discussions above, the shallow circulation increases the contrast in MSE between the dry and moist columns (not shown). Note that in this particular simulation, the radiative effect is mostly a clear-sky effect. But in similar simulations, a strong CRE-AH due to low clouds has been identified, with a similar resulting shallow circulation (Muller and Held, 2012, Muller and Bony, 2015).

Figure 3 shows regional snapshots of 925-hPa wind vectors and temperature (left panel) and precipitable water (right panel) at day 151 of a

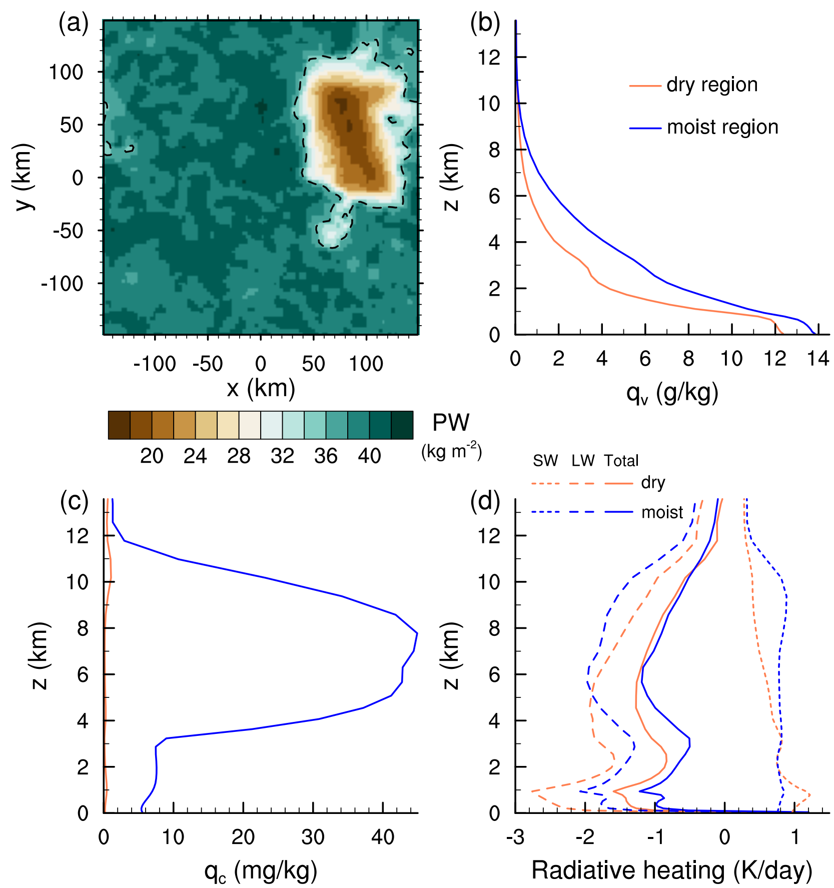

Figure 2: One-day average of a convection-permitting simulation: (a) map of precipitable water with a dashed contour showing the boundary between the moist and dry regions, (b) profile of water vapor mixing ratio, (c) profile of water condensate mixing ratio, and (d) profiles of solar (SW, dotted lines), terrestrial (LW, dashes lines) and net (total, solid lines) radiative heating rates. Blue lines refer to the moist region and red lines to the dry region.

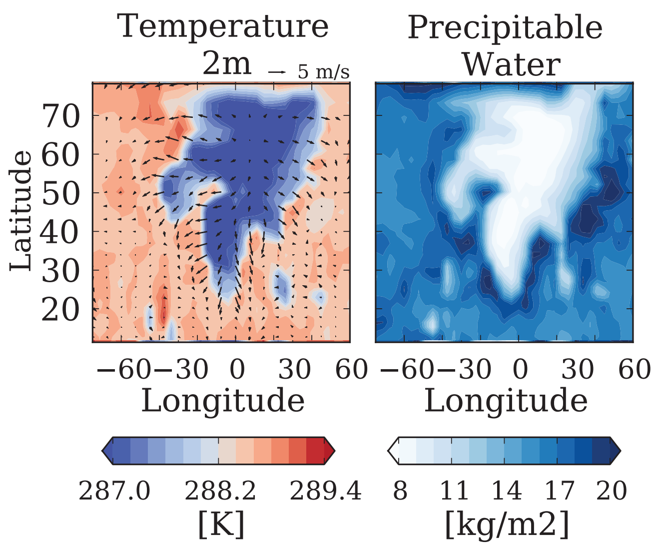

Figure 3: Radiative cold pool in a GCM simulation; left panel: temperature (shadings) and 925-hPa winds (vectors) at day 151 of the simulation; right panel: precipitable water. Adapted from Fig. 4 in Coppin and Bony (2015).

simulation using the GCM LMDz5A (Hourdin et al., 2006). The simulation was in a global radiative-convective-equilibrium configuration (i.e., without rotation and with a prescribed, uniform sea surface temperature) and initialized with horizontally uniform atmospheric conditions. In this case, the sea surface temperature is fairly low (292 K), and the spatial organization of convection results from mechanisms similar to those shown above in convection-permitting simulations. Details on the configuration and the mechanisms of self-aggregation at play in this simulation can be found in Coppin and Bony (2015). Figure 3 shows the development of a dry, cool region with near-surface winds diverging from that region. A return flow with converging winds occurs in the lower free troposphere (not shown). The expansion of this radiative cold pool eventually leads to circumscribing convection to a few limited regions of the globe.

As a final point, we note that while shallow circulations appear as a key mechanism of self-aggregation in a large number of model simulations, other mechanisms can also cause or contribute to self-aggregation (see Wing et al., 2017 for a review). Furthermore, while there are similarities between modeled self-aggregated convection and observed organized convection (see Holloway et al., 2017), it is still unclear whether the mechanisms producing self-aggregation in model simulations are active in the real world.

2.3 Observed shallow circulations

Observing systems have limited capacity to observe the three-dimensional atmospheric velocity fields and indirect estimates using diabatic heating are not robust for troposphere-deep signal, let alone shallow circulations (Bellon et al., 2017). As a result, mesoscale shallow circulations are yet to be observed.

At large scales, shallow meridional circulations (SMCs) have been identified in the tropics around tropical convergence zones. The first of such observation was in the Intertropical Convergence Zone (ITCZ) of the eastern Pacific (Zhang et al., 2004). Figure 4 shows this SMC in the boreal autumn there, with low-level flow convergence around the ITCZ, which is located at 10°–15°N in this season. The northerly cross-equatorial flow in the boundary layer converges in the ITCZ and is compensated by diverging flows both in the lower free troposphere (at 2–6 km in Fig. 4) and in the troposphere above 6 km, forming both shallow and deep overturning circulations. Similar SMCs have been observed in the central Atlantic ocean (Zhang et al., 2008) and in the Caribbean (Schulz and Stevens, 2018).

These SMCs in the ITCZ were first thought to result from the cross-

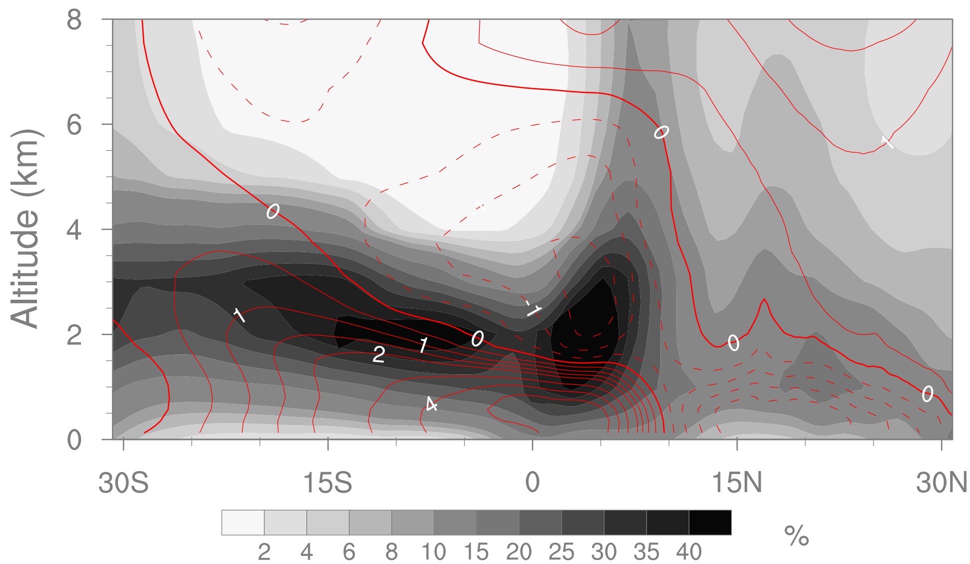

Figure 4: Cloud fraction (shadings, dataset GOCCP, Chepfer et al., 2010) and meridional wind (red contours, dataset ERA5, Hersbach et al., 2020) averaged over the eastern Pacific (90°W–120°W) in the boreal autumn (September–November).

equatorial sea surface temperature gradients that are communicated to the boundary layer air by turbulent fluxes and create pressure gradients that force the circulations (Nolan et al., 2007, 2010), but more recent work showed the role of the boundary-layer radiative cooling in the descending branch of the SMC. Figure 4 shows that the northerly flow in the non-convective region is co-located with the boundary layer clouds, which lends some credibility to a role of boundary-layer-top cooling, and particularly the CRE-AH. The SMC is also more intense if deep convection is momentarily suppressed and shallow convection is more active (Zhang et al., 2004, Yokoyama et al., 2014), potentially because the boundary-layer temperature follows more closely the sea surface temperature if deep convection is suppressed, but also because it changes the boundary-layer vertical structure and hence its radiative cooling. Additionally to the diabatic forcing, the momentum constraint allows the SMC to develop only if the ITCZ is away from the equator (Dixit and Srinivasan, 2017).

SMCs are also observed in monsoon regions such as West Africa, India, and Australia (Zhang et al., 2008, Zhai and Boos, 2017) with a rising branch over the monsoon heat low. These result from the pressure gradients between the equatorial ocean and the heat low over the continent (Zhang et al., 2008).

SMCs contribute to moistening the convergence zones, although to a lesser extent than troposphere-deep circulations. Recall from Section 2.2 that SMCs and deep circulations transport MSE in opposite directions because the vertical profile of MSE has a minimum in the lower free troposphere. On the other hand, both types of circulations import moisture into the convergence zones as water vapor decreases monotonically with height in the atmosphere (see e.g. Fig. 2b). However, by exporting air in the lower free troposphere out of the ITCZ, the ITCZ SMCs import less moisture into the ITCZ than deep circulations (Zhang et al., 2008). Monsoon SMCs even include a drying contribution from horizontal advection of moisture, which further decreases the SMCs' moistening effect: as they extend to the heat low poleward of the convergence zones, they export moist air to that region in the boundary layer while importing very dry air into the ITCZ in the lower free troposphere (Zhai and Boos, 2017).

3 Responses of tropical high clouds to the CRE-AH

This section describes the motions induced by the CRE-AH in tropical high clouds and the impacts of these motions on the evolution, lifetime, and the CRE at the TOA of these clouds. The tropical high clouds that are strongly influenced by the motions induced by their own CRE-AH include (i) cirrus in the tropical tropopause layer (TTL); these clouds form either by in-situ ice nucleation or from the remnants of anvil clouds, and (ii) anvil clouds at various stages of evolution and optical properties, ranging from very reflective fresh anvils with large ice water contents to optically thin anvils that spread far away from deep convective cores.

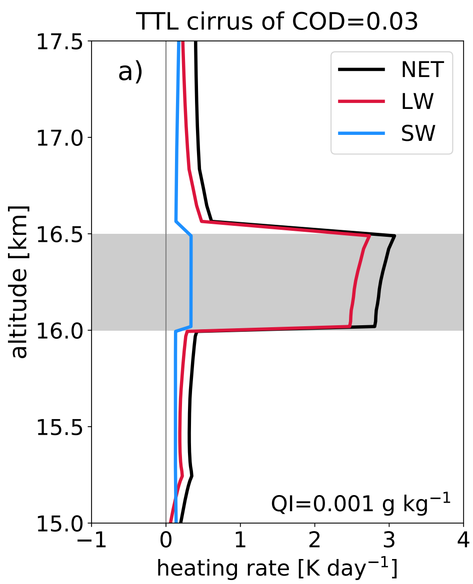

Figure 5: Radiative heating rates for a TTL cirrus assuming typical tropical temperature and moisture profiles. QI refers to ice mixing ratio. The ice crystal effective radius is set to values between 10 µm at the cloud top and 16 µm at the cloud base.

The radiative heating rates that result from the interaction of ice crystals with radiation are shown in Figs. 5 and 6 for typical high cirrus clouds. The TTL cirrus in Fig. 5 has a cloud optical depth (COD) of 0.03 and the anvil cirrus in Fig. 6 have CODs of 50, 5, and 1. The radiative heating rates shown in these figures were calculated using the Rapid Radiative Transfer Model (RRTM, Mlawer et al., 1997, Iacono et al., 2008). The absorption of LW radiation results in heating which maximizes either near the cloud top for the TTL cirrus (Fig. 5) or near the cloud bases for the anvil clouds (Fig. 6). For the thick anvil clouds that are opaque to LW radiation (Figs. 6a and b),

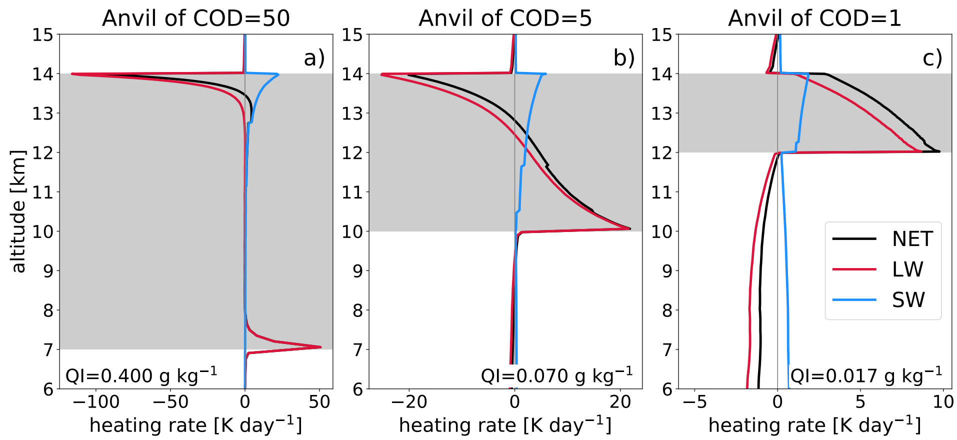

Figure 6: Radiative heating rates for (a) thick, (b) intermediately thick, and (c) thin anvil clouds assuming typical tropical temperature and moisture profiles. QI refers to ice mixing ratio. The ice crystal effective radius is set to values between 40 µm at the cloud top and 70 µm at the cloud base in case (a), 30 µm at the cloud top and 60 µm at the cloud base in case (b), and 20 µm at the cloud top and 30 µm at the cloud base in case (c), roughly in line with satellite observations of anvil clouds by Sokol and Hartmann (2020).

the large emissivities result in LW cooling near the cloud tops. For all the clouds shown, the absorption of SW radiation results in heating (Figs. 5 and 6), but the magnitude of the SW heating is significantly smaller than the LW heating and cooling.

The CRE-AH in both TTL cirrus and anvils can drive mesoscale circulations (see Figs. 1 and 7a). The circulations consist of rising vertical motions within the clouds (or portions of the clouds that are heated diabatically), compensating sinking motions outside the clouds, horizontal outflows near the cloud tops, and horizontal inflows near the cloud bases or below the levels of maximum heating (Ackerman et al., 1988, Lilly, 1988, Durran et al., 2009, Dinh et al., 2010, Gasparini et al., 2019). In addition, long exposure to a strong CRE-AH can bend the isentropic surfaces, forming unstable, convective layers within the high clouds (see Figs. 1and 7b, and also Dobbie and Jonas, 2001, Dinh et al., 2010, Schmidt and Garrett, 2013).

The magnitude and vertical profile of the CRE-AH and the corresponding dynamical responses are highly sensitive to the COD. In the following,

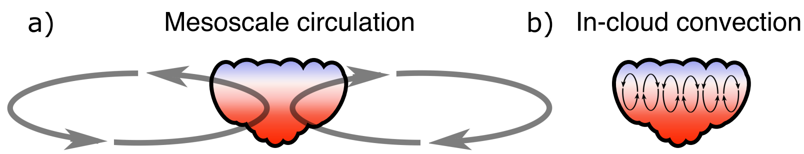

Figure 7: Air motions induced by the CRE-AH in tropical high clouds.

we therefore consider separately thin cirrus in the TTL (Section 3.1) and anvil clouds which are much thicker (Section 3.2).

3.1 TTL cirrus

Thin cirrus are widespread in the TTL, with reported cloud fractions of 20–50 % (Massie et al., 2002, Tseng and Fu, 2017). Such clouds are nearly transparent to the human eye, with CODs on the order of 0.01–0.05 (Dessler and Yang, 2003, Haladay and Stephens, 2009, Lee et al., 2009). They heat radiatively due to the absorption of LW radiation and to a minor extent SW absorption, with typical heating rates of about $5\,\mathrm{K\,d^{-1}}$ or less (Fig. 5).

TTL cirrus modulate the amount of water vapor that enters the stratosphere and therefore the radiative effect of stratospheric water vapor on climate (Dinh and Fueglistaler, 2014a). Furthermore, given that the clear-sky radiative cooling diminishes near zero in the TTL, the CRE-AH of these clouds plays a critical role in driving cross-isentropic transport of air from the TTL into the stratosphere (Corti et al., 2006, Dinh and Fueglistaler, 2014b).

The mesoscale dynamical response to the radiative heating in TTL cirrus can be qualitatively understood based on the simplied framework of a quasi-hydrostatic, two-dimensional Boussinesq fluid, for which

$$\frac{\partial b}{\partial t} + N^2 w = Q_{\mathrm{rad}}, \tag{8}$$

$$\frac{\partial u}{\partial x} + \frac{\partial w}{\partial z} = 0 \tag{9}$$

(Eqs. 3 and 4 in Durran et al., 2009). Here u and w are respectively the horizontal and vertical velocities, b is the buoyancy, N is the Brunt–Väisälä frequency, and Q_{rad} is the CRE-AH. As time goes on ($t \to \infty$),

$$w \to w_{\mathrm{ss}} = \frac{Q_{\mathrm{rad}}}{N^2}. \tag{10}$$

The steady-state vertical velocity (w_{ss}) is thus proportional to and has the same shape as the heating. Using Eq. (9) and w_{ss} in Eq. (10), the steady-state horizontal velocity can also be found. The steady-state horizontal velocity depends on the vertical gradient of the heating and extends laterally beyond the cloud/heating boundaries (Durran et al., 2009).

Following Eqs. (8) and (10), rising motions are induced in the clouds where the air is heated radiatively. Outside the lateral edges of the clouds, the buoyancy anomalies result in compensating sinking motions (see Fig. 7a and Fig. 3 in Dinh et al., 2010). Mass conservation (Eq. 9) leads to horizontal inflows in the lower halves of the cloud layers and horizontal outflows in the upper halves of the cloud layers. The developed circulations narrow the cloud bases, expand the cloud tops, and lead to the spreading and lofting of the clouds (see Figs. 6 and 7 in Dinh et al., 2010).

The mesoscale circulations described above advect environmental air into the TTL cirrus (Dinh et al., 2010, 2012, 2014). Environmental air is brought into the clouds by the inflows in the lower halves of the clouds and then advected upward by the radiatively induced rising motions in the clouds. This leads to water vapor flux convergence (divergence) inside the clouds if the ambient air is moist (dry). Therefore, depending on whether the ambient air is supersaturated or subsaturated (with respect to ice), advection of air by the mesoscale circulations supports or suppresses depositional growth of cloud ice crystals, thereby lengthening or shortening the cloud lifetime (Dinh et al., 2010, 2012, 2014).

The vertical gradient of the radiative heating is negative near the tops of the TTL cirrus (at altitude of 16.5 km in Fig. 5). This can lead to the formation of shallow unstable layers at the cloud tops that support small-scale convective motions (see Figs. 4–6 in Dinh et al., 2010). As a result, the cloud tops become heterogeneous with pockets of updrafts with higher ice water contents and areas of downdrafts mixed with environmental air leading to ice sublimation.

The relevance of the mesoscale circulations induced by the CRE-AH for TTL cirrus evolution remains disputed. In-situ measurements show that ice crystal radii are typically larger than 5–10 µm (Lawson et al., 2008, Krämer et al., 2020). Gravitational settling of large ice crystals may not allow sufficient time for the circulations to develop in response to the CRE-AH (Jensen et al., 2011). However, given that TTL cirrus can last for several days (Winker and Trepte, 1998), it is more likely than not that these in-situ observations did not sample the cloud formation period (the first 12 h or so), during which the freshly nucleated ice crystals remain small in size. The presence of wind shear and gravity wave temperature fluctuations (Dinh et al., 2016) were also shown to lead to a faster TTL cirrus decay, therefore diminishing the potential impacts of the circulations (Jensen et al., 2011, Podglajen et al., 2016). These simulations testing the roles of wind shear and temperature fluctuations were carried out for individual cloud cases only. Simulations of large cloud ensembles are needed to further investigate the sensitivity of the strength of the circulations induced by the CRE-AH to initial and environmental conditions.

3.2 Anvil clouds

The deep convective plumes of cloudy air, initially of nearly uniform potential temperature, flatten and stretch after being injected into a stably stratified environment (Lilly, 1988). The convective plumes are self-lofted by the strong latent heating within the convective updrafts until reaching the level of neutral buoyancy, which is constrained by the clear-sky radiative cooling profile (see Hartmann and Larson, 2002 and Section 1 above). The tops of the convective outflows are colder than the surrounding environment and therefore sink, while the bottoms are warmer and rise, leading to vertical compression and horizontal expansion of the convective outflows (Lilly, 1988) forming thick anvil clouds. From then on, cloud-radiative interactions start to play important roles in modulating the morphology and life cycle of anvil clouds.

As a difference from TTL cirrus, freshly detrained anvil clouds of CODs larger than about 4 develop a radiative dipole (Wall et al., 2020) characterized by LW radiative heating near cloud bases and LW cooling near cloud tops (Figs. 6a and b). The cloud tops are in addition heated by the absorption of SW radiation by the cloud condensates. The SW heating reaches comparable magnitudes to the LW cooling at the cloud tops in the middle of the day when insolation values exceeds $1000\,\mathrm{W\,m^{-2}}$ (Wall et al., 2020, Sokol and Hartmann, 2020). However, averaged over both day and night, the SW heating is of secondary importance and the net CRE-AH follows closely the LW component.

The resulting CRE-AH drives mesoscale circulations. In the simulations by Gasparini et al. (2019) shown in Fig. 8, the primary circulation includes an ascent in the middle of the cloud between 7 km and 11 km and a strong outflow at about 10–12 km (Fig. 8b). The primary circulation cell is closed

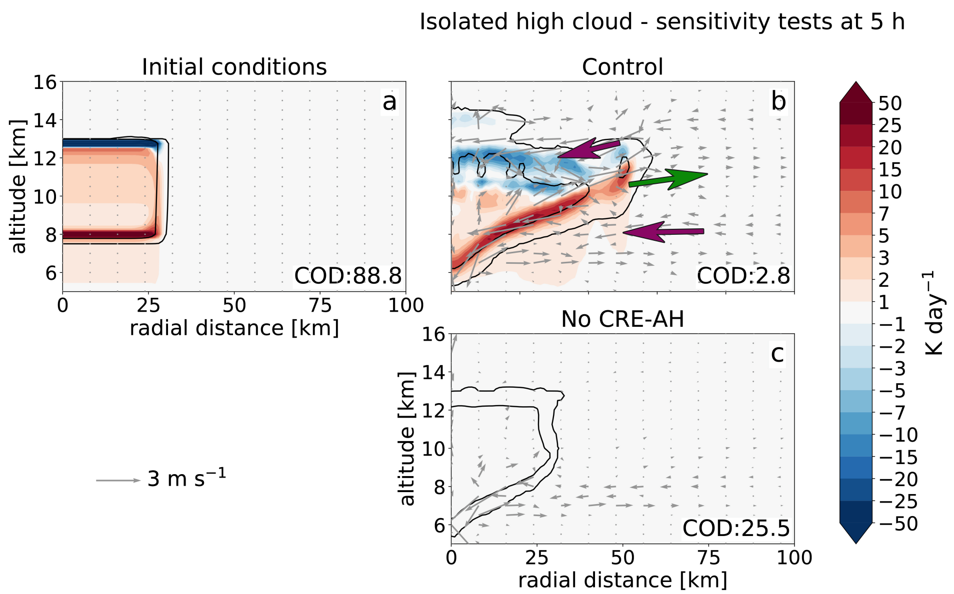

Figure 8: CRE-AH and wind vectors at (a) the initialization and (b) and (c) hour 5 after initialization of an optically thick anvil cloud simulated in a cloud-resolving model (adapted from Gasparini et al., 2019). Black contours represent ice water mixing ratios of 0.1 and 0.0001 g kg^{-1}. The vertical velocities are multiplied by a factor of 8 for a better visualization. The purple arrows highlight the inflows toward the cloud and the green arrow highlights the outflow.

by subsidence at the domain edge and an inflow at about 8–9 km altitude. The circulation spreads the upper half of the cloud and narrows the lower half of the cloud, thereby significantly changing the shape of the cloud relative to the initialization time (Fig. 8a).

Also shown in Fig. 8(b), the cloud-top radiative cooling induces downdrafts that sink the cloud top and thin the cloud. The radiative cooling further induces an inflow of drier environmental air that erodes the cloud top. This secondary circulation leads to the formation of an upper thin cirrus cloud (at about 14 km in Fig. 8b), which is later detached from the main anvil cloud. Similar clouds were observed in in-situ aircraft measurements (Garrett et al., 2004) and satellite remote sensing (Sokol and Hartmann, 2020).

Last but not least, the negative vertical gradient of the radiative heating rate (cooling above 11 km, heating below 11 km) destabilizes the air at the cloud top, resulting in convective motions and cell-like heterogeneous cloud elements there (see the $0.1\,\mathrm{g\,kg^{-1}}$ contour in Fig. 8b).

The CRE-AH strongly affects the CRE at the TOA of anvil clouds. The CRE at the TOA is the difference between the all-sky and clear-sky net (LW plus SW) incoming (downward minus upward) radiative fluxes at the TOA. In the simulations shown in Fig. 8, when the CRE-AH is turned off (Fig. 8c), the cloud at hour 5 after initialization has a COD higher than 25 and a CRE at the TOA of about $-100\,\mathrm{W\,m^{-2}}$. In contrast, in the presence of the CRE-AH (Fig. 8b), the cloud at hour 5 is optically much thinner with a COD of about 3 and a CRE at the TOA of only about $-6\,\mathrm{W\,m^{-2}}$. Integrated over the whole cloud life cycle, the net CRE at the TOA is strongly negative in the simulation without the CRE-AH, while the simulation with the CRE-AH is close to being net CRE neutral at the TOA. The latter is consistent with satellite observations that the CRE at the TOA is close to zero for tropical convective clouds over the Indo-Pacific Warm Pool (Ramanathan et al., 1989, Hartmann et al., 2001, Hartmann and Berry, 2017).

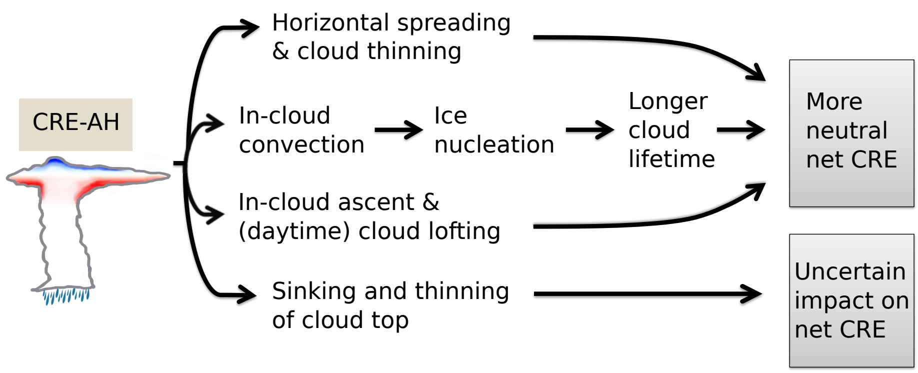

Figure 9: Mechanisms of the CRE-AH influencing the morphology and life cycle of tropical anvil clouds and their CRE at the TOA.

Figure 9 summarizes the mechanisms by which the CRE-AH of anvil clouds influences their CRE at the TOA. The dominant effect comes from the horizontal spreading of the clouds by the radiatively induced mesoscale circulations. The aging, optically thin, and horizontally extensive anvil clouds have a positive CRE at the TOA (Kubar et al., 2007, Gasparini et al., 2019), counteracting the strongly negative CRE contribution from freshly detrained, thick but much smaller anvil clouds.

The motions induced by the CRE-AH also affect the persistence and lifetime of the clouds. Within the updrafts of the small-scale convective cells at the cloud tops, nucleation of new ice crystals can take place. Freshly nucleated ice crystals are much smaller in size and therefore sediment much more slowly than the pre-existing detrained ice crystals. The matured, optically thin anvil clouds can last a long time as they are replenished with the new ice crystals at their tops. As a result, the net CRE at the TOA integrated over the entire life cycle of anvil clouds becomes more positive (Hartmann et al., 2018).

In addition, the cloud radiative heating drives in-cloud ascents, which counteract ice crystal sedimentation, prolonging the cloud lifetime. On average, the cloud radiative heating comes mainly from the LW absorption, but during the day the SW absorption can significantly increase the net heating rate (Ruppert and Hohenegger, 2018, Wall et al., 2020). Therefore, during the day, the radiatively induced updrafts can be strong enough to overcome ice crystal sedimentation, lifting the clouds to higher levels and colder temperatures, therefore exerting a stronger LW CRE at the TOA (Ruppert and Klocke, 2019, Wall et al., 2020). Finally, the LW cooling at the cloud tops leads to the sinking and erosion of the cloud tops, decreasing the lifetime of the anvil clouds. However, as the sinking and thinning of the clouds decrease both the LW and SW CRE at the TOA, the net effect on the TOA radiative fluxes is uncertain.

In summary, past observational and modeling work have highlighted the importance of the motions induced by the CRE-AH for tropical anvil clouds' evolution and radiative climatic impacts. However, we note that existing modeling studies are limited to individual cloud cases only and may not capture the full range of variation of cloud properties. Both the local CRE-AH and the CRE at the TOA of tropical high clouds are highly sensitive to the microphysical properties of ice crystals, such as their effective radius and asymmetry parameter (Järvinen et al., 2018, Bantges et al., 2020). Simulations of the tropical atmosphere in which the life cycles of a diverse cloud population are captured will be needed to thoroughly evaluate how the CRE-AH influences tropical cloud distribution and radiative effects.

References

T. P. Ackerman, K.-N. Liou, P. J. F. Valero, and L. Pfister. Heating Rates in Tropical Anvils. *J. Atmos. Sci.*, 45(10):1606–1623, 1988. doi: 10.1175/1520-0469(1988)045⟨1606:HRITA⟩2.0.CO;2.

R. J. Bantges, H. E. Brindley, J. E. Murray, A. E. Last, J. E. Russell, C. Fox, S. Fox, C. Harlow, S. J. O'Shea, K. N. Bower, B. A. Baum, P. Yang, H. Oetjen, and J. C. Pickering. A test of the ability of current bulk optical models to represent the radiative properties of cirrus cloud across the mid- and far-infrared. *Atmos. Chem. Phys.*, 20(21):12889–12903, 2020. doi: 10.5194/acp-20-12889-2020.

G. Bellon and S. Bony. Tropical and subtropical cloud systems. In *Clouds and Climate: Climate Science's Greatest Challenge*, pages 251–278. Cambridge University Press, 2020.

G. Bellon and D. Coppin. Sensitivity of convective self-aggregation to subsidence. *J. Adv. Model. Earth Syst.*, in preparation, 2021.

G. Bellon and O. Geoffroy. Stratocumulus radiative effect, multiple equilibria of the well-mixed boundary layer and transition to shallow convection. *Q. J. R. Meteorol. Soc.*, 142:1685–1696, 2016. doi: 10.1002/qj.2762.

G. Bellon, O. Reitebuch, and A. K. Naumann. Shallow circulations: Relevance and strategies for satellite observation. In *Shallow Clouds, Water Vapor, Circulation, and Climate Sensitivity*, pages 337–356. Springer, 2017.

J. W. Bergman and H. H. Hendon. Cloud radiative forcing of the low-latitude tropospheric circulation: Linear calculations. *J. Atmos. Sci.*, 57(14):2225–2245, 2000. doi: 10.1175/1520-0469(2000)057⟨2225:CRFOTL⟩2.0.CO;2.

S. Bony, B. Stevens, D. Coppin, T. Becker, K. A. Reed, A. Voigt, and B. Medeiros. Thermodynamic control of anvil cloud amount. *P. Natl. Acad. Sci.*, 113(32):8927–8932, 2016. doi: 10.1073/pnas.1601472113.

H. Chepfer, S. Bony, D. Winker, G. Cesana, J. L. Dufresne, P. Minnis, C. J. Stubenrauch, and S. Zeng. The gcm-oriented calipso cloud product (calipso-goccp). *J. Geophys. Res. Atmos.*, 115(D4), 2010. doi: 10.1029/2009JD012251.

D. Coppin and S. Bony. Physical mechanisms controlling the initiation of convective self-aggregation in a general circulation model. *J. Adv. Model. Earth Syst.*, 7(4):2060–2078, 2015. doi: 10.1002/2015MS000571.

T. Corti, B. P. Luo, Q. Fu, H. Vömel, and T. Peter. The impact of cirrus clouds on tropical troposphere-to-stratosphere transport. *Atmos. Chem. Phys.*, 6(9):2539–2547, 2006. doi: 10.5194/acp-6-2539-2006.

A. E. Dessler and P. Yang. The distribution of tropical thin cirrus clouds inferred from Terra MODIS data. *J. Climate*, 16(8):1241–1248, 2003. doi: 10.1175/1520-0442(2003)16⟨1241:TDOTTC⟩2.0.CO;2.

T. Dinh and S. Fueglistaler. Microphysical, radiative and dynamical impacts of thin cirrus clouds on humidity in the tropical tropopause layer and stratosphere. *Geophys. Res. Lett.*, 41:6949–6955, 2014a. doi: 10.1002/2014GL061289.

T. Dinh and S. Fueglistaler. Cirrus, Transport, and Mixing in the Tropical Upper Troposphere. *J. Atmos. Sci.*, 71:1339–1352, 2014b. doi: 10.1175/JAS-D-13-0147.1.

T. Dinh and S. Fueglistaler. Mechanism of Fast Atmospheric Energetic Equilibration Following Radiative Forcing by CO_2. *J. Adv. Model. Earth Syst.*, 9, 2017. doi: 10.1002/2017MS001116.

T. Dinh and S. Fueglistaler. On the Causal Relationship between the Moist Diabatic Circulation and Cloud Rapid Adjustment to Increasing CO_2. *J. Adv. Model. Earth Syst.*, 11, 2019. doi: 10.1029/2019MS001853.

T. Dinh, D. R. Durran, and T. Ackerman. Cirrus and water vapor transport in the tropical tropopause layer – Part 1: A specific case modeling study. *Atmos. Chem. Phys.*, 12(20):9799–9815, 2012. doi: 10.5194/acp-12-9799-2012.

T. Dinh, S. Fueglistaler, D. Durran, and T. Ackerman. Cirrus and water vapour transport in the tropical tropopause layer – Part 2: Roles of ice nucleation and sedimentation, cloud dynamics, and moisture conditions. *Atmos. Chem. Phys.*, 14(22):12225–12236, 2014. doi: 10.5194/acp-14-12225-2014.

T. Dinh, A. Podglajen, A. Hertzog, B. Legras, and R. Plougonven. Effect of gravity wave temperature fluctuations on homogeneous ice nucleation in the tropical tropopause layer. *Atmos. Chem. Phys.*, 16:35–46, 2016. doi: 10.5194/acp-16-35-2016.

T. P. Dinh, D. R. Durran, and T. P. Ackerman. Maintenance of tropical tropopause layer cirrus. *J. Geophys. Res. Atmos.*, 115(D2):1–15, 2010. doi: 10.1029/2009JD012735.

V. Dixit and J. Srinivasan. The momentum constraints on the shallow meridional circulation associated with the marine itcz. *Meteorol. Atmos. Phys.*, 129(6):595–609, 2017. doi: 10.1007/s00703-016-0489-2.

S. Dobbie and P. Jonas. Radiative influences on the structure and lifetime of cirrus clouds. *Q. J. R. Meteorol. Soc.*, (127):2663–2682, 2001. doi: https://doi.org/10.1002/qj.49712757808.

D. R. Durran, T. Dinh, M. Ammerman, and T. Ackerman. The Mesoscale Dynamics of Thin Tropical Tropopause Cirrus. *J. Atmos. Sci.*, 66(9): 2859–2873, 2009. doi: 10.1175/2009jas3046.1.

S. Fermepin and S. Bony. Influence of low-cloud radiative effects on tropical circulation and precipitation. *J. Adv. Model. Earth Syst.*, 6(3):513–526, 2014. doi: 10.1002/2013MS000288.

T. J. Garrett, A. J. Heymsfield, M. J. McGill, B. A. Ridley, D. G. Baumgardner, T. P. Bui, and C. R. Webster. Convective generation of cirrus near the tropopause. *J. Geophys. Res. Atmos.*, 109(21):1–14, 2004. doi: 10.1029/2004JD004952.

B. Gasparini, P. N. Blossey, D. L. Hartmann, G. Lin, and J. Fan. What drives the life cycle of tropical anvil clouds? *J. Adv. Model. Earth Syst.*, 11(8):2586–2605, 2019. doi: 10.1029/2019MS001736.

I. B. Glenn and S. K. Krueger. Connections matter: Updraft merging in organized tropical deep convection. *Geophys. Res. Lett.*, 44(13):7087–7094, 2017. doi: 10.1002/2017GL074162.

J. M. Gregory, W. J. Ingram, M. A. Palmer, G. S. Jones, P. A. Stott, R. B. Thorpe, J. A. Lowe, T. C. Johns, and K. D. Williams. A new method for diagnosing radiative forcing and climate sensitivity. *Geophys. Res. Lett.*, 31(3):L03205, 2004. doi: 10.1029/2003GL018747.

T. Haladay and G. Stephens. Characteristics of tropical thin cirrus clouds deduced from joint cloudsat and calipso observations. *J. Geophys. Res. Atmos.*, 114(D8), 2009. doi: 10.1029/2008JD010675.

D. L. Hartmann and S. E. Berry. The balanced radiative effect of tropical anvil clouds. *J. Geophys. Res. Atmos.*, 122, 2017. doi: 10.1002/2017JD026460.

D. L. Hartmann and K. Larson. An important constraint on tropical cloud-climate feedback. *Geophys. Res. Lett.*, 29(20):10–13, 2002. doi: 10.1029/2002GL015835.

D. L. Hartmann, L. A. Moy, and Q. Fu. Tropical convection and the energy balance at the top of the atmosphere. *J. Climate*, 14(24):4495–4511, 2001. doi: 10.1175/1520-0442(2001)014⟨4495:TCATEB⟩2.0.CO;2.

D. L. Hartmann, B. Gasparini, S. E. Berry, and P. N. Blossey. The life cycle and net radiative effect of tropical anvil clouds. *J. Adv. Model. Earth Syst.*, 10(12):3012–3029, 2018. doi: 10.1029/2018MS001484.

J. M. Haynes, T. H. Vonder Haar, T. L'Ecuyer, and D. Henderson. Radiative heating characteristics of Earth's cloudy atmosphere from vertically resolved active sensors. *Geophys. Res. Lett.*, 40(3):624–630, 2013. doi: 10.1002/grl.50145.

H. Hersbach, B. Bell, P. Berrisford, S. Hirahara, A. Horányi, J. Muñoz-Sabater, J. Nicolas, C. Peubey, R. Radu, D. Schepers, A. Simmons, C. Soci, S. Abdalla, X. Abellan, G. Balsamo, P. Bechtold, G. Biavati, J. Bidlot, M. Bonavita, G. De Chiara, P. Dahlgren, D. Dee, M. Diamantakis, R. Dragani, J. Flemming, R. Forbes, M. Fuentes, A. Geer, L. Haimberger, S. Healy, R. J. Hogan, E. Hólm, M. Janisková, S. Keeley, P. Laloyaux, P. Lopez, C. Lupu, G. Radnoti, P. de Rosnay, I. Rozum, F. Vamborg, S. Villaume, and J.-N. Thépaut. The era5 global reanalysis. *Q. J. R. Meteorol. Soc.*, 146(730):1999–2049, 2020. doi: 10.1002/qj.3803.

C. E. Holloway, A. A. Wing, S. Bony, C. Muller, H. Masunaga, T. S. L'Ecuyer, D. D. Turner, and P. Zuidema. Observing convective aggregation. In *Shallow Clouds, Water Vapor, Circulation, and Climate Sensitivity*, pages 26–63. Springer, 2017. doi: 10.1007/s10712-017-9419-1.

Y. Hong, G. Liu, and J.-L. F. Li. Assessing the radiative effects of global ice clouds based on cloudsat and calipso measurements. *J. Climate*, 29(21): 7651–7674, 2016. doi: 10.1175/JCLI-D-15-0799.1.

F. Hourdin, I. Musat, S. Bony, P. Braconnot, F. Codron, J.-L. Dufresne, L. Fairhead, M.-A. Filiberti, P. Friedlingstein, J.-Y. Grandpeix, et al. The lmdz4 general circulation model: climate performance and sensitivity to parametrized physics with emphasis on tropical convection. *Clim. Dyn.*, 27(7-8):787–813, 2006. doi: 10.1007/s00382-006-0158-0.

M. J. Iacono, J. S. Delamere, E. J. Mlawer, M. W. Shephard, S. A. Clough, and W. D. Collins. Radiative forcing by long-lived greenhouse gases: Calculations with the AER radiative transfer models. *J. Geophys. Res. Atmos.*, 113(13):2–9, 2008. doi: 10.1029/2008JD009944.

E. Järvinen, O. Jourdan, D. Neubauer, B. Yao, C. Liu, M. O. Andreae, U. Lohmann, M. Wendisch, G. M. McFarquhar, T. Leisner, and M. Schnaiter. Additional global climate cooling by clouds due to ice crystal complexity. *Atmos. Chem. Phys.*, 18(21):15767–15781, 2018. doi: 10.5194/acp-18-15767-2018.

E. J. Jensen, L. Pfister, and O. B. Toon. Impact of radiative heating, wind shear, temperature variability, and microphysical processes on the structure and evolution of thin cirrus in the tropical tropopause layer. *J. Geophys. Res. Atmos.*, 116(12):1–9, 2011. doi: 10.1029/2010JD015417.

M. Krämer, C. Rolf, N. Spelten, A. Afchine, D. Fahey, E. Jensen, S. Khaykin, T. Kuhn, P. Lawson, A. Lykov, L. L. Pan, M. Riese, A. Rollins, F. Stroh, T. Thornberry, V. Wolf, S. Woods, P. Spichtinger, J. Quaas, and O. Sourdeval. A microphysics guide to cirrus – Part 2: Climatologies of clouds and humidity from observations. *Atmos. Chem. Phys.*, 20(21):12569–12608, 2020. doi: 10.5194/acp-20-12569-2020.

T. L. Kubar, D. L. Hartmann, and R. Wood. Radiative and convective driving of tropical high clouds. *J. Climate*, 20(22):5510–5526, 2007. doi: 10.1175/2007JCLI1628.1.

C. Lac, J.-P. Chaboureau, V. Masson, J.-P. Pinty, P. Tulet, J. Escobar, M. Leriche, C. Barthe, B. Aouizerats, C. Augros, P. Aumond, F. Auguste, P. Bechtold, S. Berthet, S. Bielli, F. Bosseur, O. Caumont, J.-M. Cohard, J. Colin, F. Couvreux, J. Cuxart, G. Delautier, T. Dauhut, V. Ducrocq, J.-B. Filippi, D. Gazen, O. Geoffroy, F. Gheusi, R. Honnert, J.-P. Lafore, C. Lebeaupin Brossier, Q. Libois, T. Lunet, C. Mari, T. Maric, P. Mascart, M. Mogé, G. Molinié, O. Nuissier, F. Pantillon, P. Peyrillé, J. Pergaud, E. Perraud, J. Pianezze, J.-L. Redelsperger, D. Ricard, E. Richard, S. Riette, Q. Rodier, R. Schoetter, L. Seyfried, J. Stein, K. Suhre, M. Taufour, O. Thouron, S. Turner, A. Verrelle, B. Vié, F. Visentin, V. Vionnet, and P. Wautelet. Overview of the Meso-NH model version 5.4 and its applications. *Geosci. Model Dev.*, 11(5):1929–1969, 2018. doi: 10.5194/gmd-11-1929-2018.

J. P. Lafore, J. Stein, N. Asencio, P. Bougeault, V. Ducrocq, J. Duron, C. Fischer, P. Héreil, P. Mascart, V. Masson, J. P. Pinty, J. L. Redelsperger, E. Richard, and J. Vilà-Guerau de Arellano. The Meso-NH Atmospheric Simulation System. Part I: adiabatic formulation and control simulations. *Ann. Geophys.*, 16(1):90–109, 1998. doi: 10.1007/s00585-997-0090-6.

K. Larson and D. L. Hartmann. Interactions among cloud, water vapor, radiation, and large-scale circulation in the tropical climate. Part I: Sensitivity to uniform sea surface temperature changes. *J. Climate*, 16(10): 1425–1440, 2003. doi: 10.1175/1520-0442-16.10.1425.

R. P. Lawson, B. Pilson, B. Baker, Q. Mo, E. Jensen, L. Pfister, and P. Bui. Aircraft measurements of microphysical properties of subvisible cirrus in the tropical tropopause layer. *Atmos. Chem. Phys.*, 8:1609–1620, 2008. doi: 10.5194/acp-8-1609-2008.

J. Lee, P. Yang, A. E. Dessler, B.-C. Gao, and S. Platnick. Distribution and radiative forcing of tropical thin cirrus clouds. *J. Atmos. Sci.*, 66(12):3721 – 3731, 2009. doi: 10.1175/2009JAS3183.1.

Y. Li, D. W. J. Thompson, and S. Bony. The Influence of Atmospheric Cloud Radiative Effects on the Large-Scale Atmospheric Circulation. *J. Climate*, 28(18):7263–7278, 2015. doi: 10.1175/JCLI-D-14-00825.1.

D. K. Lilly. Cirrus outflow dynamics. *J. Atmos. Sci.*, 45(10), 1988. doi: 10.1175/1520-0469(1988)045⟨1594:COD⟩2.0.CO;2.

S. Massie, A. Gettelman, W. Randel, and D. Baumgardner. Distribution of tropical cirrus in relation to convection. *J. Geophys. Res.*, 107(D21):4591, 2002. doi: 10.1029/2001JD001293.

E. J. Mlawer, J. Taubman, P. D. Brown, M. J. Iacono, and S. A. Clough. Radiative transfer for inhomogeneous atmospheres: RRTM, a validated correlatedk model for the longwave. *J. Geophys. Res.*, 102(D14):16663–16682, 1997. doi: doi:10.1029/97JD00237.

C. Muller and S. Bony. What favors convective aggregation and why? *Geophys. Res. Lett.*, 42(13):5626–5634, 2015. doi: 10.1002/2015GL064260.

C. J. Muller and I. M. Held. Detailed investigation of the self-aggregation of convection in cloud-resolving simulations. *J. Atmos. Sci.*, 69(8):2551–2565, 2012. doi: 10.1175/JAS-D-11-0257.1.

A. K. Naumann, B. Stevens, C. Hohenegger, and J. P. Mellado. A conceptual model of a shallow circulation induced by prescribed low-level radiative cooling. *J. Atmos. Sci.*, 74(10):3129–3144, 2017. doi: 10.1175/JAS-D-17-0030.1.

A. K. Naumann, B. Stevens, and C. Hohenegger. A moist conceptual model for the boundary layer structure and radiatively driven shallow circulations in the trades. *J. Atmos. Sci.*, 76(5):1289–1306, 2019. doi: 10.1175/JAS-D-18-0226.1.

D. S. Nolan, C. Zhang, and S.-H. Chen. Dynamics of the shallow meridional circulation around intertropical convergence zones. *J. Atmos. Sci.*, 64(7): 2262–2285, 2007. doi: 10.1175/JAS3964.1.

D. S. Nolan, S. W. Powell, C. Zhang, and B. E. Mapes. Idealized simulations of the intertropical convergence zone and its multilevel flows. *J. Atmos. Sci.*, 67(12):4028–4053, 2010. doi: 10.1175/2010JAS3417.1.

A. Podglajen, R. Plougonven, A. Hertzog, and B. Legras. A modelling case study of a large-scale cirrus in the tropical tropopause layer. *Atmos. Chem. Phys.*, 16(6):3881–3902, 2016. doi: 10.5194/acp-16-3881-2016.

V. Ramanathan, R. D. Cess, E. F. Harrison, P. Minnis, B. R. Barkstrom, E. Ahmad, and D. Hartmann. Cloud-Radiative Forcing and Climate: Results from the Earth Radiation Budget Experiment. *Science*, 243(4887): 57–63, 1989. doi: 10.1126/science.243.4887.57.

D. A. Randall, Harshvardhan, D. A. Dazlich, and T. G. Corsetti. Interactions among Radiation, Convection, and Large-Scale Dynamics in a General Circulation Model. *J. Atmos. Sci.*, 46(13):1943–1970, 1989. doi: 10.1175/1520-0469(1989)046⟨1943:IARCAL⟩2.0.CO;2.

J. H. Ruppert and C. Hohenegger. Diurnal circulation adjustment and organized deep convection. *J. Climate*, 31(12):4899–4916, 2018. doi: 10.1175/JCLI-D-17-0693.1.

J. H. Ruppert and D. Klocke. The two diurnal modes of tropical upward motion. *Geophys. Res. Lett.*, 46:2911–2921, 2019. doi: 10.1029/2018GL081806.

M. Saint-Lu, S. Bony, and J. L. Dufresne. Observational Evidence for a Stability Iris Effect in the Tropics. *Geophys. Res. Lett.*, 47(14), 2020. doi: 10.1029/2020GL089059.

C. T. Schmidt and T. J. Garrett. A simple framework for the dynamic response of cirrus clouds to local diabatic radiative heating. *J. Atmos. Sci.*, 70(5):1409–1422, 2013. doi: 10.1175/JAS-D-12-056.1.

T. Schneider, P. A. O'Gorman, and X. J. Levine. Water vapor and the dynamics of climate change. *Rev. Geophys.*, 48:RG3001, 2010. doi: 10.1029/2009RG000302.

H. Schulz and B. Stevens. Observing the tropical atmosphere in moisture space. *J. Atmos. Sci.*, 75(10):3313–3330, 08 2018. ISSN 0022-4928. doi: 10.1175/JAS-D-17-0375.1.

A. Slingo and J. M. Slingo. The response of a general circulation model to cloud longwave radiative forcing. I: Introduction and initial experiments. *Q. J. R. Meteorol. Soc.*, 114(482):1027–1062, 1988. doi: 10.1002/qj.49711448209.

J. M. Slingo and A. Slingo. The response of a general circulation model to cloud longwave radiative forcing. II: Further studies. *Q. J. R. Meteorol. Soc.*, 117(498):333–364, 1991. doi: 10.1002/qj.49711749805.

A. Sokol and D. L. Hartmann. Tropical anvil clouds: Radiative driving towards a preferred state. *Earth and Space Science Open Archive*, page 28, 2020. doi: 10.1002/essoar.10503124.2.

D. W. J. Thompson, S. Bony, and Y. Li. Thermodynamic constraint on the depth of the global tropospheric circulation. *P. Natl. Acad. Sci.*, 114(31): 8181–8186, 2017. doi: 10.1073/pnas.1620493114.

B. Tian and V. Ramanathan. A simple moist tropical atmosphere model: The role of cloud radiative forcing. *J. Climate*, 16(12):2086–2092, 2003. doi: 10.1175/1520-0442(2003)016⟨2086:ASMTAM⟩2.0.CO;2.

H.-H. Tseng and Q. Fu. Tropical tropopause layer cirrus and its relation to tropopause. *J. Quant. Spectrosc. Ra.*, 188:118–131, 2017. doi: 10.1016/j.jqsrt.2016.05.029.

C. J. Wall, J. R. Norris, B. Gasparini, W. L. Smith Jr., M. M. Thieman, and O. Sourdeval. Observational Evidence that Radiative Heating Modifies the Life Cycle of Tropical Anvil Clouds. *J. Climate*, 33:8621–8640, 2020. doi: 10.1175/JCLI-D-20-0204.1.

J. M. Wallace and P. V. Hobbs. *Atmospheric science: an introductory survey*, volume 92. Elsevier, 2006.

A. A. Wing, K. Emanuel, C. E. Holloway, and C. Muller. Convective self-aggregation in numerical simulations: A review. In *Shallow Clouds, Water*

Vapor, Circulation, and Climate Sensitivity, pages 1–25. Springer, 2017. doi: 10.1007/978-3-319-77273-8_1.

D. M. Winker and C. R. Trepte. Laminar cirrus observed near the tropical tropopause by LITE. *Geophys. Res. Lett.*, 25(17):3351–3354, 1998. doi: 10.1029/98GL01292.

R. Wood. Stratocumulus clouds. *Mon. Wea. Rev.*, 140(8):2373–2423, 2012. doi: 10.1175/mwr-d-11-00121.1.

J.-I. Yano, W. W. Grabowski, and M. W. Moncrieff. Mean-State Convective Circulations over Large-Scale Tropical SST Gradients. *J. Atmos. Sci.*, 59 (9):1578–1592, 2002. doi: 10.1175/1520-0469(2002)059⟨1578:MSCCOL⟩2.0.CO;2.

C. Yokoyama, E. J. Zipser, and C. Liu. Trmm-observed shallow versus deep convection in the eastern pacific related to large-scale circulations in reanalysis datasets. *J. Climate*, 27(14):5575–5592, 2014. doi: 10.1175/JCLI-D-13-00315.1.

M. D. Zelinka and D. L. Hartmann. Why is longwave cloud feedback positive? *J. Geophys. Res.*, 115(D16):D16117, 2010. doi: 10.1029/2010JD013817.

J. Zhai and W. R. Boos. The drying tendency of shallow meridional circulations in monsoons. *Q. J. R. Meteorol. Soc.*, 143(708):2655–2664, 2017. doi: 10.1002/qj.3091.

C. Zhang, M. McGauley, and N. A. Bond. Shallow meridional circulation in the tropical eastern Pacific. *J. Climate*, 17(1):133–139, 2004. doi: 10.1175/1520-0442(2004)017⟨0133:SMCITT⟩2.0.CO;2.

C. Zhang, D. S. Nolan, C. D. Thorncroft, and H. Nguyen. Shallow meridional circulations in the tropical atmosphere. *J. Climate*, 21(14):3453–3470, 2008. doi: 10.1175/2007JCLI1870.1.